IAC–19–A6,IP,20,x53728

AI to Support Decision Making in Collision Risk Assessment

Luis Sánchez[a]*, Massimiliano Vasile[a], Edmondo Minisci[a]

[a]*Department of Mechanical & Aerospace Engineering,University of Strathclyde, James Weir Building, 75 Montrose Street, Glasgow, United Kingdom G11XJ*,
luis.sanchez-fdez-mellado@strath.ac.uk
*Corresponding Author

Abstract

This paper introduces an Artificial Intelligence(AI)-based system to support operators to manage the risk of collisions. The system implements an Artificial Neural Network (ANN) based technique to predict the risk of collision between two space objects, where one of the two is an operational satellite and the other one is a piece of space debris. The ANN based technique provides a prediction of the Probability of Collision (P_C), MOID and B-parameter between a primary satellite and a set of space debris objects during an interval of time starting from a database including the initial states synthetic space objects. Results of the system over a database of synthetic objects not previously seen during training show the good accuracy predicting the evolution of the aforementioned variables. The achieved results suggest that the proposed system can be able to implement in collision assessment as a method to identify - quickly, accurately and automatically - possible conjunctions between space objects in a interval of time with no use of dynamic models or orbit propagators. A revised calculation of the P_C is also proposed to mitigate the Dilution of Probability that affects the usual definition of this quantity. This phenomenon gives the counterintuitive idea that the lower the quality of the data (or amount of information available to the operators), the smaller the probability of collision, which can lead to a false confidence in the likelihood of a collision or forces operators to accept very large margins. The method presented here will account for epistemic uncertainty under the assumption of Dempster-Shaffer's Theory of Evidence which leads to the definition of confidence intervals on the probability of a collision. Confidence interval incorporate the dependency of the probability of collision on the amount and quality of the available information, using the concepts of Belief and Plausibility introduced in Theory of Evidence. The result of this revised calculation of the P_C is a more informed decision. At the same time, a lack of information can lead to a higher uncertainty on the decision to be made. Thus the paper will propose a possible approach to make optimal decisions under epistemic uncertainty where the cost of the decision is the risk associated to the decision are concurrently taken into account.

Keywords: Neural Networks, Space Traffic Management, Probability of Collision, Evidence Theory

1. Introduction

The number of Space Resident Objects (RSO) has experienced a continuous growth since the beginning of the space era. Currently, ESA (European Space Agency) quantifies in more than $20,000$ just the number of trackable objects in orbit, of which only 10% are operational satellites [1], not taking into account those objects small enough not to be detected. Moreover, during the next decades, a number of mega-constellation with thousand of satellites each [2] are expected to be deployed, which have to be added to the increasing number of small satellites [3] put in orbit. Neither of them were expected on the model of the space environment evolution implemented some years ago, which already predicted an increase on the number of both satellites and space debris objects. This means that the total number of operational satellites will increase on the following years by a factor of three times or more with respect to current predictions [4]. Taking into account the expected increase on the number of potential operative satellites and the current space debris objects, the space environment for the future years will be highly populated. So far, there have been some important events (collisions and collision avoidance maneuver, CAM) involving operative satellites and pieces of space debris, like the collision of an Iridium satellite and the Cosmos 2251 satellite on February 2009 [5]. Moreover, also encounters between operational satellites has been recorded, for example, the recently first CAM performed by ESA to avoid a collision with a new mega-constellation satellite on September 2019. [6]

A more populated space environment means that similar

events will be more likely in the future and stress the importance to have a robust and updated Space Traffic Management (STM) system . The IAA (International Academy of Astronuatics) Cosmic Study on Space Traffic Management defined STM as "the set of technical and regulatory provisions for promoting safe access into outer space, operations in outer space and returns from outer space to Earth free from physical or radio-frequency interference". In this, conjunction risk assessment is a key factor, especially considering the very high increase on the number of RSO's expected within the coming years. Therefore, new techniques should be incorporated on the decision making process to help operators to perform conjunction risk assessment. Artificial Intelligence (AI) techniques have been used on engineering problems on the recent years. Some of them implement Support Vector Machine [7], others Elastic Net [8] among others. More examples can be found here [9]. ANNs have also been applied to orbit position prediction [10] that show the availability of this sort of techniques.

What is proposed in this paper is using an ANN based system to automatize and speed up the evaluation of the collision risk among operative satellites and space debris, using a database with initial parameters. The ANN system is able to provide the Minimum Orbital Intersection Distance (MOID), B-parameter and Probability of Collision (P_C) along an interval of time between an operative satellite and a piece of space debris. The system needs, as inputs, the initial orbital parameters of both bodies, and does not need any propagator.

In addition to the new techniques to improve the prediction of conjunctions events, STM needs a trustworthy metric to evaluate the risk of collision. Currently, Probability of Collision (P_C) is widely used by operators in conjunction analysis and its use is granted and never questioned [11, 12, 13]. However, the use of P_C suffers the so called *dilution* effect, that is a reduction on the value of probability of collision when the relative position of the two objects is poorly determined, (Pc has been *diluted* to a low level through high uncertainties in the objects' state estimates), leading to a false confidence on the operator's decisions. Considering also the risk associated with an increase on space population, an alternative method to evaluate the risk of collision on a conjunction events is proposed here. This new formulation considers the epistemic uncertainty on the conjunction analysis (mean reason below probability dilution [14]) and, using Dempster-Shafer's Theory of Evidence (DST) [15], provides upper and lower bounds for the confidence of a value of probability of collision, based on the evidence provided by the sources of information.

The rest of the paper is structured as follows. In Section 2, an introduction to ANN is presented, focusing on those relevant aspect or the system presented here. Section 3 introduces the structure of the system, while Section 4 presents the results obtained when the proposed ANN-based system has been applied to a study case scenario. Section 5 delves in the concepts of probability of dilution, Theory of Evidence and includes same example to illustrate the new method proposed. Finally, Section 6, summarizes the ideas proposed in the paper and suggests future research and application steps.

2. Neural Network Background

One of the capabilities enabled by Machine Learning (ML) algorithms is to build a model, based on data sets (training data), of a process in order to make predictions without running the process itself, which can be hidden or can be expensive to reproduce or run. ML can be used also to reconstruct the functional relationship between a set of input and a set of output data. In this section we propose the use of ML to build a global model of the collision risk between a given space asset and all the objects in a given orbit regime. The orbit regime is identified by a range of possible orbital parameters.

Generic Multi-Layer Perceptron (MLP) Feed-Forward Artificial Neural Networks (FF-ANN) with one hidden layer are used to learn the initial equinoctial parameters of space debris objects, and infer the equinoctial parameters for future epochs. Many hidden layers can be used, but for this problem one layer is enough. Single layer MLPs are universal function approximators $\mathbf{f_g}(\mathbf{x}) : \mathbb{R}^{n_d} \rightarrow \mathbb{R}^{n_o}$ [16], where n_d is the size of the input vector $\mathbf{x}$, and n_o is the size of the output vector function $\mathbf{f_g}$. In the present version, $\mathbf{x} = (\mathcal{X}_0)^T$, where $\mathcal{X}_0$ is the vector of equinoctial parameters at the initial time, and $n_d = 6$, whereas $n_o = 1$ since the output function is scalar, corresponding to one of the equinoctial parameters in a future epoch. A more detailed explanation about the structure of the ANN used here is presented in Section 3. The general matrix-vector definition of $\mathbf{f_g}$ is:

$$\mathbf{f_g}(\mathbf{x}) = A_2(\mathbf{b}^{(2)} + \mathbf{W}^{(2)}(A_1(\mathbf{b}^{(1)} + \mathbf{W}^{(1)}\mathbf{x}))) \qquad (1)$$

where $\mathbf{W}^{(1)}$ is a weight matrix of size $(N \times n_d)$ and N is the number of neurons in the hidden layer, $\mathbf{b}^{(1)}$ is a bias (column) vector of length N, $\mathbf{W}^{(2)}$ is a weight matrix of size $(n_0 \times N)$, $\mathbf{b}^{(2)}$ is a bias (column) vector of length n_o, and $A1$ and $A2$ are the activation functions of the hidden layer and the output layer respectively.

The activation function of the hidden layer, A_1 can be selected among a set of functions, such as sigmoid, hyperbolic tangent sigmoid function, reLU [17]. For this model,

$A1$ has been chosen to be the hyperbolic tangent sigmoid function defined as $tanh(a) = (e^a - e^{-a})/(e^a + e^{-a})$. A_2, due to being a regression problem has to be a linear (eq. 2.

$$\mathbf{f_g}(\mathbf{x}) = \mathbf{b}^{(2)} + \mathbf{W}^{(2)}(tanh(\mathbf{b}^{(1)} + \mathbf{W}^{(1)}\mathbf{x})) \qquad (2)$$

Given a set of N_s training samples $\{(\mathbf{x}_1, \mathbf{y}_1), \ldots, (\mathbf{x}_{N_s}, \mathbf{y}_{N_s})\}$, where $\mathbf{y}_i$ is the observed response to the input $\mathbf{x}_i$, a learning algorithm seeks the values of the weight matrices and bias vectors that minimise the difference between the observed N_s sample responses $\mathbf{y}_i$ and the N_s responses given by $\mathbf{f_g}(\mathbf{x}_i)$. Gradient-based optimization is often used to determine the weight matrices and the bias vectors. If the responses $\mathbf{x}_i$ are smooth functions of their inputs and the internal weights and biases, the gradients with respect to weights and biases of the difference of the sample responses and their approximations can be computed using the back-propagation procedure, which basically relies on applying the chain rule for derivation. Thus, the components of the gradient of the objective function with respect to the input of a layer can be computed by working backwards from the gradient with respect to the output of that module (or the input of the subsequent module). The back-propagation approach can be applied repeatedly to propagate gradients through all layers starting from the output at the top, where the network gives its response, and working all the way down to the bottom, where the input is provided. Once the gradients with respect to weights and biases for each layer are computed, the objective function expressing the level of fitting of the training data can be optimised.

Since the different inputs can vary on very different scales (from thousands of km in the case of semimajor axis, to 10-100 for L and 10^{-3} for P_1, P_2, Q_1, Q_2), the values for each of the features should be scale to a common interval in order to equate the effect of each one.

If the ANNs system has a sufficiently high number N of degrees of freedom (or neurons) in the hidden layer, the fitting error can be reduced to machine zero, but this usually implies that the system may overfit the training data, and be unable to generalize adequately its predictions in regions of the input space where there are no training data [18]. To mitigate this risk, following approach has been adopted in this study. Subdividing the available data set into a training set and a test set. At each step of the gradient-based optimisation via backpropagation (training), the fitting error based on the test set is also computed. The system training is then stopped when the fitting error based on the test set starts increasing. This typically happens before the fitting error based on the training set achieves machine zero.

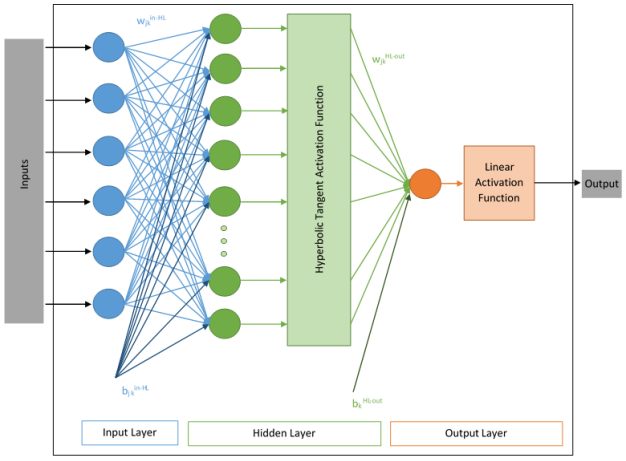

Fig. 1: General structure of the proposed ANNs.

Using this learning approach to prevent overfitting, the learning process via back-propagation corresponds to a local gradient-based optimisation method which is solved with the Levenberg-Marquardt method [19]. Because of the local nature of the method, however, the learning outcome can be affected by the process initialisation. To reduce the likelihood of this occurrence, a number of training runs with different random initializations are carried out. Moreover, different values of N can be tested to determine the value that optimizes the trade-off of prediction reliability and computational cost of the learning process. In this study, the size of the training set is 80% of the randomised database and that of the test set is 20% of the same database. An additional 10% has been used for the validation set, used after the training process, to check the behaviour of the already trained network over samples not seen previously.

The ANNs system selected for the corresponding equinoctial parameter at the corresponding future time is that with the better fitting of the training set and the better generalization on the test set. The typical value of N determined for the different equinoctial parameters of the ANNs system varies between 60 and 500, although in this paper only results with 200 neurons has been used for speeding the training stage, leaving for future works the optimize selection of N for each of the ANNs used in the model.

3. Neural Network model

With the proposed ANN based approach, it is possible to obtain a meta-model of the movement of the secondary satellite, which can then be used to compute, during a certain interval of time, the risk of collision evolution between an primary space object and a secondary one, without the need of any orbital propagator. Two main consequences of

the use of the proposed ANN based approach are a reduction of the computational time, and the possibility to perform the analysis without the use of a dynamical model.

A considerable reduction of the computational time is expected, because, once the ANN has been trained, no orbital propagator is used and the ANN gives the evolution of the orbital parameters in a fraction of a second. Moreover, if more than one piece of debris is analysed, the computational time that can be saved further increases. On the other hand, if the model is trained using a database of real satellites data, no error associated with the dynamical models is introduced in the outcomes, reducing the sources of errors to those that the observational data already included. However, this second aspect is not considered in this work, since the database used to feed the model is a synthetic one, where virtual satellites are created and propagated using a high fidelity propagator simulation against the ANN predictions are compared as the "true" values.

3.1 Model description

The method proposed in this paper allows the computation of the evolution of the risk of probability between a primary body, considered as an operational satellites, and one ore more secondaries bodies or space debris objects. In order to achieve that, a set of ANN models are created to predict the equinoctial elements of the secondary object along a certain period of time and, thus, compute the evolution of MOID, B-parameter and probability of collision (P_C) or any other measurement of the risk of conjunction.

The method uses an AI based system composed by: one section where the ANN surrogate model is used to compute the equinoctial parameters of the secondary object, and a second part where the risk of collision metric is computed - in this case, the new Evidence Theory based probability of collision is considered.

The first part is where the AI techniques are used, consisting on a set of "6 x Number_of_trainable_epochs" ANNs. These ANN are trained at certain epochs ("trainable epochs") inside the interval of interest. Thus, time is not longer needed to be predict, allowing the decouple of the orbital parameter prediction from the time variable. Although it leads to a bigger number of ANN to be trained, also they are simpler. At each of those trainable epochs, six ANN are trained to predict each of the six equinoctial parameters of the secondary object. A lineal interpolation method is used to obtain the equinoctial elements for times different than trainable epochs, using the two ANN trained at the closest epochs.

The second part of the system takes the outcomes of the ANNs, i.e. the equinoctial parameters of the secondary object, and, using the propagated orbit of the primary object, computes the variable related with the risk of conjunction between the two bodies.

The simulation environment used to create the model has some simplification and assumptions:

- The primary body is assumed to have completely known movement.
- The second satellites is assumed to be moving following a perturbed movement, under the effect of the Earth gravitational harmonics, third body (Moon and Sun), drag and solar radiation pressure.
- The secondary satellites' true movement is obtained by propagating the initial state with the a high fidelity propagator in C++ developed at Aerospace Center of Excellence (ACE) of the University of Strathclyde.
- The ANN are trained with a dataset of virtual space objects whose initial orbital parameters are included in a certain range of values. This means that, due to the reduced extrapolation capacity of ANN [20], the final trained networks only work for new objects with initial data included on those intervals.
- The epoch at which the orbital parameter for the primary and the secondary object are given, must be the same. This epoch is considered as the initial time ($t_0 = 0$) for the ANN surrogate model.
- During the ANN phase (both, training and prediction) the time variable used is not the actual epoch associated to the orbital parameters, but elapsed time from the initial epoch at which the orbital parameters are provided. It allows to predict any new object's equinoctial parameters by just adding the elapsed time given by the ANN to it initial epoch.

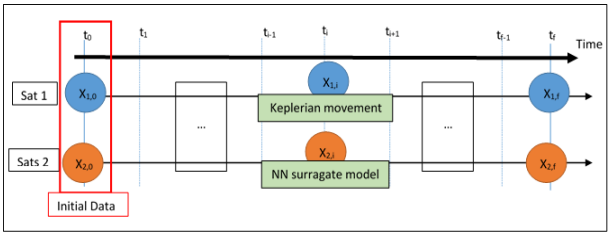

Fig. 2: Simulation environment flowchart for the ANN model.

3.2 Database

A synthetic database that contains data of a set of space debris objects in Low Eart Orbit, LEO, has been considered.

To create this database, an certain number of satellites have been generated, provided their initial state/parameters, randomly distributed within certain ranges of values, at a common initial epoch. This initial parameters are propagated along the interval of interest and afterwards, the equinoctial parameters at each time-step are computed from the propagated Keplerian elements / Cartesian coordinates for each of the satellites. A database, including all the satellites for all the trainable epochs, is generated from this data as a matrix containing on each row: a) the initial equinoctial parameters for the corresponding object, b) the equinoctial parameters at a certain epoch, and c) the elapsed time.

As mentioned in Section 2, three subsets should be created for training, testing and validation. A 10% of randomly chosen satellites are extracted from this table in order to validate the trained model with no previously seen data. Note that the separated data are not just a random 10% sample set of the samples, but a 10% of the satellites, so that when validating a reconstruction of the evolution of the orbit (and consequently, the risk of collision) can be made using just unseen data.

Once these two dataset are obtained, they are divided again into the smaller datasets that have actually to be used during the training stage. This subdivision it is made according the structure of the ANN model: six small dataset, one per each equinoctial parameter, are generated per each epoch the ANNs are going to be trained at. Each of these datasets includes: the six initial equinoctial parameters for each satellite and the corresponding orbital element the ANN that used this dataset is going to predict at the corresponding epoch (Table 1).

Table 1: Generic example of a dataset at epoch_j to predict the equinoctial parameter_k.

Dif epoch_j ($t_j - t_0$)		
# Sat_2	**Initial equinoctial parameters**	**Equinoctial parameter**$_k$ **at** t_j
Sat2_1	$\mathcal{X}_{10}$	$\mathcal{X}_{k1j}$
Sat2_2	$\mathcal{X}_{20}$	$\mathcal{X}_{k2j}$
...	...	...
Sat2_i	$\mathcal{X}_{i0}$	$\mathcal{X}_{kij}$

These datasets are the ones that have been used to train the ANNs at the basis of the surrogate model. Each of these small datasets contains as many rows as satellites used for training and 7 columns: the first 6 are the features used as inputs for the ANN (the six initial equinoctial elements) and the last one the "real" value used to supervise the learning process (the equinoctial element to be predicted of the corresponding satellite at that time).

Equinoctial elements have to be preferred to other orbital parameters or the state vectors for a number of reasons. First, state vector is changing value fast although periodically. This high frequency variance on its values leaded a more challenging set of variable to predict what usually meant a better prediction. On the other hand, equinoctial elements are much more flat, variation are mainly long term ones and a slightly bad prediction of the short term frequency has a smaller impact on the computation of their variables as MOID, B-parameter and P_C. Secondly, although the Keplerian elements have been used to define the range of values among which the initial orbital state of the space debris can be comprised to, they are not used due to the angular nature of most of its elements. This variables suffer bigger variation on its values, specially near circular orbits, where the argument of perigee, since it is not defined in circular orbits, suffer drastic variation on its values that the ANN struggle to predict. However, equinoctial elements are non-singular elements, so their values doesn't suffer from that variation when the orbits are close to circular, equatorial or polar. Furthermore, the only angular variable is the true longitude, that is always increasing, so the ANN should not experienced further problem in its prediction.

Finally, as it was mentioned before, the reason why several time independent ANN has been trained instead of one including the time is due to the different nature of the variables. When including the time among the predictable variables, the behaviour of the other, periodic on its nature, was understood by the ANN as noise and just the long term variation were predicted, averaging the short term oscillations. Since in this problem, not just the general trend, but the possible extremes values are important (since P_C occur for the small values of B-parameter), this approach was discarded.

3.3 Neural network structure

Each of the previous databases are used to train a ANN predicting the equinoctial parameters of a space debris object, given its initial parameters. Combining the six ANN trained for each epoch, it is possible to reconstruct the state of the satellite, and repeating the process for each epoch over which the ANN is trained, it is possible to obtain the evolution of the orbit along the period of time of interest.

The structure of each ANN is similar: one input layer with six neurons corresponding to the six initial equinoctial elements, one output layer giving the prediction of the equinoctial element and one single hidden layer.

The ANN model has been implemented using the MATLAB *Deep Learning* Toolbox. The training process has

been configured to allow the selection and setting of the value of different ANN hyperparameters, such as: the number of nodes per hidden layer, the number of epochs of training, optimizer using during the backpropagation and its hyperparameters, the cost function, and activation function of the neurons of each layer.

3.4 Conjunction metrics: MOID, B-parameter and Pc

The second part of the system uses the data predicted by the ANNs to obtain the evolution and final values of new parameters related with the risk of collision: MOID, B-parameter and the probability of collision.

The MOID (Minimum Orbit Intersection Distance) is the minimum distance between two osculating orbits and is used as a measure of the risk of collision between two objects. Since it contains information just about the orbits, but not about the position of the satellite on the orbit, a low MOID is a signal of possible collision but it does not guarantee the conjunction is going to happen. Since in the model, the secondary object is considered to follow a perturbed motions, the osculating orbit is not fixed, so it is necessary to compute the MOID at each step of time. More details about the MOID calculation and its implementation can be found in [21] and [22].

It is referred as B-parameter the norm of the vector that goes from the one of the bodies, considered as the target, and the other, when the second intersects the so call B-plane or Body Plane [23, 24]. The B-parameter defined this way is equivalent to the miss distance used in the computation of the probability of collision by different authors [11, 12, 13]. The B-plane is usually defined for hyperbolic orbits, as the plane containing the centre of mass of the target orbit and perpendicular to the asymptote, or equivalently, normal to the velocity in the infinity. Since in this paper the relative velocity of the orbits near the conjunction is considered to be rectilinear, as a common assumption on conjunction analysis studies [13], the B-plane can be alternatively defined as the plane perpendicular to the relative velocity centered on the target object, that is considered to be the primary object. Opposite as the MOID, the B-parameter actually gives direct information about the proximity of the two satellites, means that a value of the B-parameter close to zero means that both orbits are in an encounter trajectory (as long as the uncertainty on the position is not considered). To compute the B-parameter it is necessary to know the relative velocity vector between both bodies and the position of both objects, in order to compute the B-plane coordinates and eventually the B-parameter. To do so, a previous transformation from equinoctial parameters to Cartesian coordinates is needed. Since the B-parameter depends on the actual position of both satellites on its orbit, it had been computed at every time step. However, since B-parameter is a metric used when a conjunction happens, only those values close to zero makes actual sense. Nevertheless, this is not a problem since a high probability of collision is associated with a low value of the B-parameter.

Finally, the probability of collision is the actual metric used by operator to evaluate the risk of collision and decide if further measures are needed in order to avoid it. Although it is related with the miss distance between both objects or the B-parameter (as it is described in this paper), the P_C accounts for the uncertainty on the measure of the bodies' position. In Section 5 more information about the current P_C computation methods can be found.

4. Case of study

On this section a study case where the AI/based system explained on the previous sections is shown. The results are compare with those obtain with the high fidelity propagator, whose results are considered here as the "true values".

4.1 Initial data

In the Table 2 are summarized the scenario of the simulation for the present study case. The interval of time to make predictions and detect possible conjunctions is 1 day since the initial epoch which the data are provided at. A set of six ANN are trained each 400 seconds since the initial along the whole interval. For the entire scenario, 775 objects have been created, simulating pieces of space debris. Among those samples, 75 have been chosen for the validation dataset and the other 700 have been used for training, splitting them into training dataset and test dataset in a ratio of 80-20%, respectively, plus a 10% used for validation. The databases have been generating from the initial parameters provided at an epoch 7/03/2019 12:00:00 UT (2458550 JD) and randomly distributed along the range of values included on the Table 3. The propagation of these orbits have been made using the aforementioned high fidelity propagator (in C++ language) developed by ACE of University of Strathclyde. Propagation time was 1 day, time step 400 seconds and the perturbations considered: Earth gravity field, Drag, Third Body and Solar Radiation Pressure. Once the orbit were propagated, the keplerian elements at each propagation time were converted to equinoctial elements. The propagated equinoctial elements are considered as the true values for this study.

During the training process, a total of 1296 ANNs have been created (six each 400 seconds during 1 day) using the Neural Net Fitting app of Matlab's Deep Learning Toolbox.

Table 2: Summarize of the scenario.

Parameter	Value
Prediction interval time (days)	1
Time step for training (s)	400
Total number of samples	775
Number of training dataset samples	560
Number of test dataset samples	140
Number of validation dataset samples	75

Table 3: Range of initial orbital parameter of the secondary objects.

Initial epoch	7/03/2019 12:00:00 UT
Range of values for orbital parameters	
Semimajor axis (km)	7000 - 7100
Eccentricity	0.0001 - 0.001
Inclination (deg)	70 - 90
RAAN (deg)	0 - 20
Argument of perigee (deg)	0 - 20
True Anomaly (deg)	0 - 20

The parameters used for the training in this scenario have been selected after a previous analysis to find a good combination of them. Nevertheless, a detailed study on the effect of the combination of the hyperparameters on the results of the prediction for this problem is suggested as a future work. All the ANN has the same structure, summarize on Table 4. Only 1 hidden layer with 200 nodes has been needed. Each of these neurons has an hyperbolic tangent sigmoid activation function. The only output layer neuron uses a lineal activation function since this is a regression problem. The optimizer used during the backpropagation have been Levenberg-Marquardt. The cost function to be optimized was the Mean Squared Error (MSE):

$$MSE = \frac{1}{N}\sum_{i=1}^{N}(Y_i - \hat{Y}_i)^2 \tag{3}$$

where Y_i is the real value of the sample's output and $\hat{Y}_i$ is the outcome of the ANN for the same sample.

The maximum number of epochs per training was 10,000. The value of the thresholds depended on the equinoctial parameter: the threshold for the cost function value for the semimajor axis was 10^{-5}, and for the other parameters 10^{-11}, the value of the gradient for the cost function was 10^{-7}, and the number of epochs where the cost function over the test data is not any longer improving was 6. Each ANN is trained 10 times with the same combination

Table 4: Summarize of the scenario.

Parameter	Value
Number of hidden layers	1
Neuron in hidden layer	200
Activation Func.	Hyperbolic tangent
Maximum number of epochs	10,000
Cost function value threshold	10^{-5} - 10^{-11}
Cost function gradient threshold	10^{-7}
Num. epoch not improving thresh.	6
Optimizer	Levenberg-Marquardt
Cost function	MSE
Number of iterations	10

Table 5: Primary satellite initial orbital parameters.

Initial epoch	7/03/2019 12:00:00 UT
Parameters	**Value**
Semimajor axis (km)	7.08861703e+03
Eccentricity	1.01712114e-03
Inclination (deg)	8.00546778e+01
RAAN (deg)	1.11921004e+01
Argument of perigee (deg)	1.48650152e+02
True anomaly (deg)	2.79347844e+02

of hyperparameters, changing the initialization of weights and bias and the distribution of the training and test datasets.

The orbital parameters of the primary satellite can be found on the Table 5 and have been selected to ensure at least one close encounter with at least one of the examples included on the validation database during the interval of interest.

4.2 Results

A summarize with the performance of the trained ANNs can eb seen in Table 6. The table shows the percentage of samples predicted by the ANN fall inside the $\pm$ 5% and $\pm$ 1% error intervals for training and validation databases.

For the training dataset, it can be seen the high values of samples with errors smaller than 1% and 5% for the prediction of equinoctial elements, bigger than 95% for all cases, less P_1 and P_2. This result can be expected, since these samples are the same used during training process, what gives and idea of the fitting capabilities of the ANNs. Regarding the B-parameter and MOID, not directly predicted by the ANN, the percentages are high (even if P_1 and P_2 do not present high values accuracy), since they are obtain from the predicted equinoctial parameters.

Table 6: Percentage of samples below 1% and 5% error for training and validation datasets.

	Training [%] ($\pm$1% - $\pm$5%)	**Validation [%]** ($\pm$1% - $\pm$5%)
Equinoctial parameters (a, P_1, P_2, Q_1, Q_2, L)	100.0 - 100.0 24.74 - 34.93 58.48 - 68.49 96.84 - 96.98 100 - 100 99.97 - 99.99	100.0 - 100.0 15.32 - 27.48 30.55 - 54.57 81.84 - 84.69 100.0 - 100.0 99.18 - 99.99
MOID	83.42 - 95.41	69.16 - 90.18
B-parameter	99.99 - 100.0	99.42 - 99.95

More interesting is the column regarding the validation database samples. This results shows the capacity of the ANNs to generalize the trends recognized during training to data not seen before, that it is exactly the situation they are expected to work in. It can be seen that prediction of equinoctial parameters remains in high values of percentage of samples inside the 1% and 5% intervals, greater than 80% or even close to 100%, for almost all the parameters. Despite r than in training case, presenting lower accuracy than training results, as expected, they are still really close to them. Only P_1 and P_2 show low values of accuracy, but at it can be seen, it does not propagate to B-parameter or MOID. Figure 3 gives and idea of the distribution of prediction. The prediction values lies over the diagonal representing real values for a, Q_1, Q_2 and L, as expected from the table, and also for P_2. P_1 shows a higher dispersion near values close to 0. This gives and idea how well ANNs can generalize for this problem and how them can be used to replace orbital propagators when speed is needed.

The values for MOID and B-parameter shows also good results. In the case of B-parameter, results are near 100% of error less than 5%, what means that it heritages the good performances on the prediction of equinoctial parameters and shows how the errors on P_1 and P_2 do not influence the prediction of this variable. In the case of MOID, results are slightly lower. The reason of this worse numbers can be seen from Figure 4. It shows the real values versus predicted values for MOID and B-parameter, as well as the evolution of those variables for one of the samples included in the validation dataset. The evolution of MOID change more randomly and its values are closer to zero than for B-parameter, what explain the worse prediction: rapid changes are harder to predict and since it is closer to zero, the effect of the bad prediction of P_1 has more influence. Nevertheless, the trend in both cases is very well predicted.

From this results, it can be said that ANNs can be used for conjunction risk assessment with obtaining good accuracy with good computational cost performances. However, considering a situation where a conjunction actually occurs, Figure 5, it can be seen that the error between real and predicted value is too big: 6km for predicted value versus 0km the real one. Under this new consideration, ANN are still a good tool for conjunction risk assessment, but in another way: from Figures 4 and 5, it is shown that ANNs predict better the trend that exact values when they are close to zero, so instead of using them as a tool to obtain exact value for B-parameter to be used in the P_C computation, they can be used to filter potential conjunction events. In this way, the potential conjunction events of one satellite with several space debris objects can be obtain rapidly with no propagator, and then, used a dedicated tool to establish the actual risk for those potential situations.

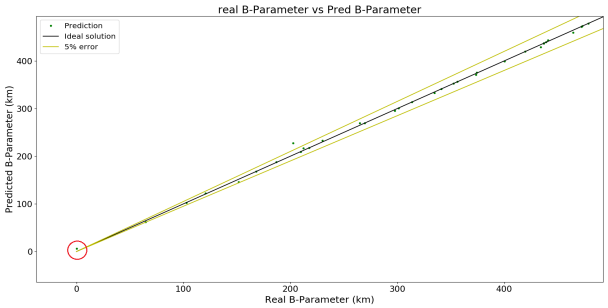

Fig. 5: Detail of real B-parameter versus predicted B-parameter for the conjunction case. Red circle: conjunction event: real value = 0km, predicted value = 6km.

Due to the fact that the Probability of Collision, P_C,for nearly all the cases evaluated during the training and validations is zero, no results regarding the probability of collision are presented in this section. Nonetheless, the probability of collision is directly related with B-parameter, e.g. miss distance (see eq. 4 in 5), and taking into account no effects on the uncertainty have been consider so far in this work, the results obtained for the evolution of B-parameter and the potential conjunctions can be easily translated to the evolution of P_C.

Once seen the good performances on the ANN model for predicting equinoctial parameters and obtaining the B-parameter and probability of collision, a new method to evaluate the risk of conjunction based on the Theory of Evidence is presented in the next section.

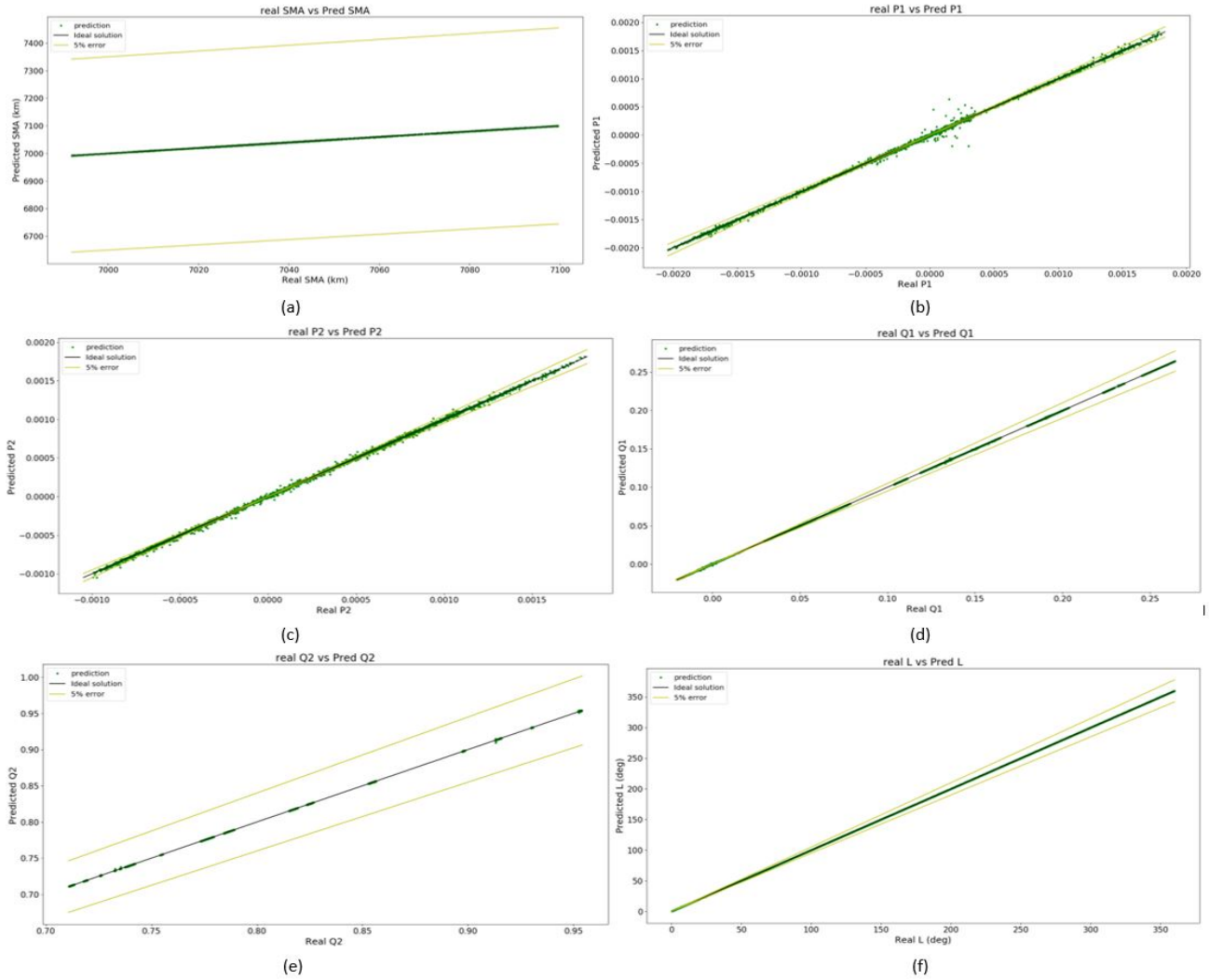

Fig. 3: Equinoctial parameters: real value versus predicted value over all the sample on validation dataset. Green dots: predictions; black line: ideal solution; yellow lines: $\pm 5\%$error.

5. Collision Risk Under Epistemic Uncertainty

5.1 Dilution of Probability

The probability of collision (P_c) is a common metric to evaluate the risk of collision between two space objects. Its value depends on the uncertainty on position, velocity and dynamics of the two objects. If the value P_c is greater than a given threshold, then a collision avoidance manoeuvre or any other action should be triggered. The most popular methods for computing the Probability of Collision are based on the calculation of an integral of a probabilistic distribution over a bounded region, or a simplification of that integral [11, 12, 13]. Often P_c is computed under the following assumptions defining a fast encounter [12]:

- Relative motion is considered rectilinear.
- Positional errors have zero-mean, are Gaussian, and uncorrelated.
- Covariances in velocity are assumed zero due to short duration of the encounter.
- The objects are modelled as hard spheres.

Thanks to this simplifying assumptions, the probability distributions of the positions of the two objects, which are

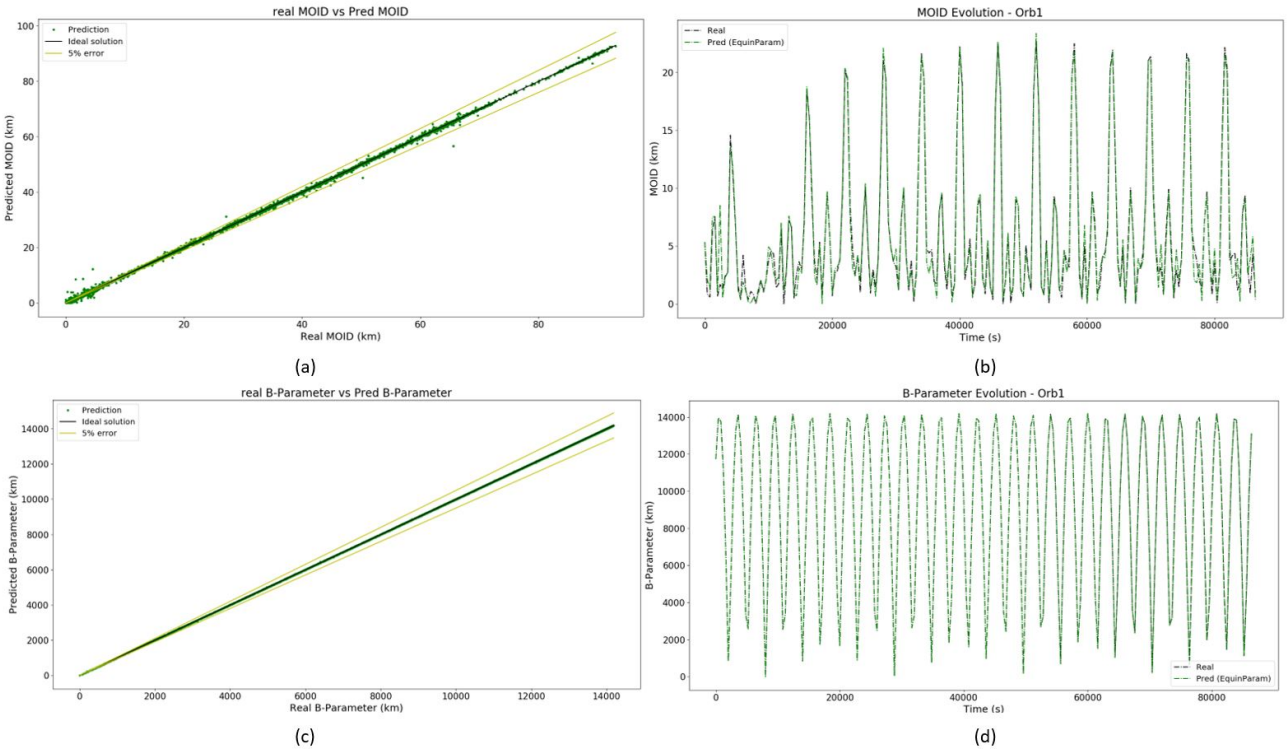

Fig. 4: (a) MOID real vs MOID predicted values over all validation samples. (b) MOID evolution between primary satellite and one space debris object. (c) B-parameter real vs B-parameter predicted values over all validation samples. (d) B-parameter evolution between primary satellite and one space debris object.

generally assumed to be unimodal and Gaussian, can be combined into a single uncertainty ellipsoid around one of the bodies, and projected onto the associated impact plane (or B-Plane). The calculation of P_c translates into the computation of an integral in two dimensions, where the integration of the projected covariances has to be made over the bounded regions delimited by the intersection of the combine body sphere with the intersection plane.

$$P_C = \frac{1}{2\pi\sigma_x\sigma_y} \int\limits_{\mathcal{B}((0,0),R)} exp\left(-\frac{1}{2}\left(\frac{(x-\mu_x)^2}{\sigma_x^2} + \frac{(y-\mu_y)^2}{\sigma_y^2}\right)\right) dxdy \quad (4)$$

where μ_x and μ_x are the miss distances (x and y components) between the two objects, σ_x and σ_y are the combine positional uncertainty and the $\mathcal{B}((0,0),R)$ is the integration region. The integration region is the sphere enveloping the spheres representing the two objects: hard body radius (HBR).

Although broadly used by operators [25], the P_c leads to a paradoxical phenomenon known as dilution of probability [12, 26]. The dilution of probability gives a decreasing probability of collisions as the uncertainty on the position of the two objects increases. The reason is that an increase in uncertainty is translated into an increase in σ (see Figure 6) regardless of the nature of the uncertainty. Since position uncertainty gives an idea of the data quality, a decrease of epistemic probability of collision when increasing the uncertainty, i.e. lower quality data, seems counter-intuitive. [14]

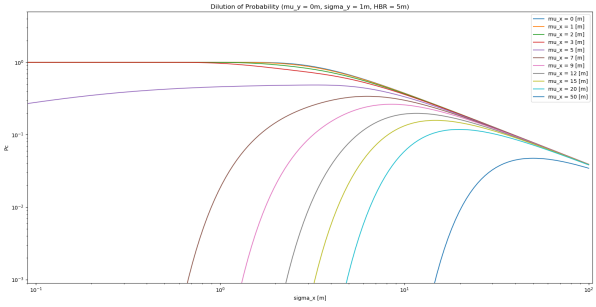

Fig. 6: Probability of dilution as a function of σ_x for different values of μ_x. $HBR = 5m$, $\sigma_y = 1m$, $\mu_y = 0m$.

As shown in [14], the mathematics underneath the com-

putation of the probability of collision is quite straightforward but the model of uncertainty is not. In fact, if one assumed that the process was purely aleatory, as the quality of the data decreases, one would correctly expect that the collision probability also would decrease. This conclusion would require a perfect knowledge of dynamics and sensors so that the probability associated to an event is exactly known. However, if the quality of the data is due to a lack of knowledge or incomplete information, one would come to the conclusion that ignorance is bliss because a reduced knowledge on the state of the objects would lead the operators to believe that there is a low risk of a collision(see Figure 7 for a 1D example).

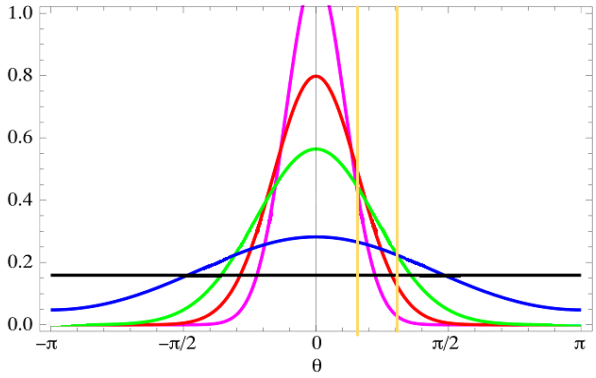

Fig. 7: The bounded region between the vertical yellow lines and below the pink curve is smaller than the area below the red or green curves, which have a bigger standard deviation. It means an increase on the P_c. However, if the increasing on the standard deviation continues (curves blue and black) the bounded area becomes smaller due to the flatten on the Gaussian pdf, leading to the dilution of probability.

The lack of knowledge or incomplete information are classified as epistemic uncertainty. Thus one can argue that a more complete and sensible treatment of the probability of collision should assume that the uncertainty in the state and dynamics of space objects is not completely aleatory. Epistemic uncertainty can be a better model for positional uncertainty on conjunction analysis and can incorporate partial knowledge of the true dynamics. When the P_c is recalculated incorporating epistemic uncertainty, its value is associated to a degree of belief in the quality of the observations and thus a reduction of the probability of collision has to be interpreted in the light of the actual information available to the operator.

In this section, we take a first step towards the calculation of a collision metric that accounts for both epistemic and aleatory uncertainty. We maintain the assumptions of fast collision and the Gaussian model for the P_c but we assume that mean and variance are affected by epistemic uncertainty deriving from the quality of the data. We then model this epistemic uncertainty with Dempster-Shafer Theory of Evidence, and we associate a degree of belief to the realisation of a particular collision probability.

Note that a more complete treatment would drop the assumption of Gaussian distribution and would include epistemic uncertainty also in the dynamics and not simply in the observation data. In the remainder of the paper, however, we limit ourselves only to some simple but illustrative examples to demonstrate the importance of the correct treatment of epistemic uncertainty.

5.2 Theory of Evidence

A key aspect of this work is that uncertainty in observations is deemed to be epistemic in nature and cannot be quantified by precise probability distributions. In order to capture this imprecision and lack of knowledge the use of Dempster-Shafer Theory of Evidence is proposed. DST has been used in other engineering problems to model uncertainty with good results [27, 28, 15]. The fact that DST can associate a degree of belief in the realisation of a given event without a precise quantification of the probability of that event to occur is exploited. It is assumed that the sources of information for each parameter are independent and uncertainties are uncorrelated, as it is considered in DST. This assumption is reasonable in most of the cases related with this paper.

Given an event space, the set Θ of all the mutually exclusive and collectively exhaustive elementary events (or hypotheses) $\Theta = \left\{\theta_1, \theta_2, ..., \theta_i, ..., \theta_{|\Theta|}\right\}$ is considered. The different available sources of evidence are treated independently in this paper.

The collection of all non empty subsets of Θ is the Power Set $2^\Theta = (\Theta, \cup)$.One can now assign a probability mass, called basic probability assignment (bpa), to the elements of 2^Θ. Each element of 2^Θ with a non-zero bpa is called a *Focal Element* (FE) and is represented with the symbol γ in the following. The pair $\langle \Gamma, bpa_\Gamma \rangle$ - where $\Gamma \ni \gamma$ and $bpa_\Gamma \ni bpa_\gamma$ - is called the *Body of Evidence*. The power set $U = 2^\Theta$ the *Uncertain Space* in this work. It is possible now define the performance index of the system to be analysed as:

$$f(\mathbf{u}) : U \subseteq \mathbb{R}^m \rightarrow \mathbb{R} \tag{5}$$

where U the event space for the uncertain parameters $\mathbf{u}$, of dimension m.

DST measures the influence of uncertainty on the quantity f by means of two functions, *Belief* and *Plausibility*, that generalise the concept of Probability measure given in

classical probability theory. The following set can be define to show the amount of evidence associated to an event:

$$\Omega = \{\mathbf{u} \in U | f(\mathbf{d}, \mathbf{u}) \in \Phi\} \tag{6}$$

as the corresponding set in U and then compute the cumulative Belief and Plausibility associated to that event:

$$Bel(\Omega) = \sum_{\gamma_i \subset \Omega, \gamma_i \in U} bpa(\gamma_i), \tag{7}$$

$$Pl(\Omega) = \sum_{\gamma_i \cap \Omega \neq \emptyset, \gamma_i \in U} bpa(\gamma_i). \tag{8}$$

From Eqs. (7) and (8) it can be stated that the belief in the realisation of the event $f(x) \in \Phi$ is the sum of the bpa of all the FEs totally included in Ω, while the Plausibility is the sum of all the FEs that have a non-null intersection with Ω. Furthermore, it can be said that the Belief is the amount of positive support a proposition have accumulate from the evidence while the Plausibility is the lack of evidence against the proposition. More details about the DST can be found in [15].

5.3 New Formulation of the Risk of Collision

In this section we introduce the assumption that the quality of data can be modelled with DST and affects the mean and the variance of the Gaussian distributions associated to the position of a given object. In other words, the value of mean and variance can belong to one or more focal elements and we can assign a belief value to each of them. The result is a degree of belief and plausibility associated to each Probability of Collision. The difference between Belief and Plausibility is a confidence interval on that P_c and define the lower and upper bounds on the confidence that the operator should have in the occurrence of a collision.

We start by assuming that different experts provide intervals for mean and variance and we are able to associate a degree of belief to each interval. We maintain the assumption of uncorrelated and independent sources for the sake of simplicity of presentation of our arguments although this assumption can be easily relaxed. The intervals provide by the different experts should be combine before building the Uncertain Space using any combination rule as explain later.

The Cartesian product of all these intervals obtained after the combination of sources forms the frame of discernment Θ, from which we build the Uncertain Space $U = 2^{\Theta}$. An example of Uncertain Space for two variables, $\mu_x - \sigma_x$ can be found in Figure 8. Each of the regions built up from the intervals for each variable is a Focal Element, γ, which has an associated bpa. conforming the Body of Evidence.

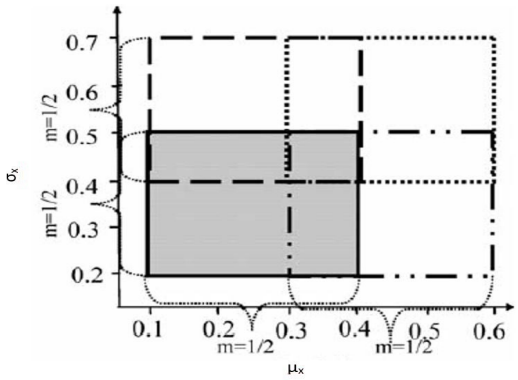

Fig. 8: Uncertain space for 2D case. μ_x intervals: [0.1,0.4] and [0.3,0.6], σ_x intervals: [0.2,0.5]and [0.4,0.7]. The bpa for all the intervals is 0.5. The for delimited boxes (Cartesian product) constitute the Focal Elements. [29]

Once the body of evidence of evidence is set up, it is possible to compute the Plausibility and Belief functions of the probability of collision being bigger than a certain value. Using eq. 4, it can be obtain the maximum and minimum value of the probability of collision associated to each Focal Element, from which the bpa is taken. To obtain the Plausibility and Belief functions, a slightly modification on formulation is done, to obtain confidence of being bigger than a certain value instead of being smaller, that is what eqs. 8 and 7 provide. The modified equation are:

$$Bel(P_C > P_{C_0}) = 1 - \sum_{P_{C_{max}}(\gamma_i) > P_{C_0}} bpa(\gamma_i) \tag{9}$$

$$Pl(P_C > P_{C_0}) = 1 - \sum_{P_{C_{min}}(\gamma_i) > P_{C_0}} bpa(\gamma_i) \tag{10}$$

where γ_i in eqs. 9 and 10 are the Focal Elements whose maximum and minimum value of P_C is bigger or smaller than P_{C_0} , respectively.

Combination rules

A previous step for the building of the Uncertain Space, is the combination of the assessment of the same variable (intervals from experts) for the different sources of information, what is known as combination rules on the DST. There are several combination rules that mainly differ on the on the way they deal with conflict information sources, more information can be found in [30]. Since the selection of the combination rule has an impact on the intervals and bpas used to build the Uncertain Space and, in consequence, with the final Belief and Plausibility curves, an illustrative example is presented here to compare two different rules and to

understand the effect on the final results depending on the characteristics of the evidences.

The combination rules selected are Dempster Rule and Mixing Rule, due to the different result they usually give under conflict sources, and they are compared over two scenarios. Since one of the main differences among combination rules is the way they deal with conflict information, the scenarios present a high and low level of conflict, respectively. In this context, conflict between sources of information refers to the fact that the intervals provides by them mainly overlap (low conflict) or present a small fraction in common (high conflict).

Dempster Rule is the original combination rule proposed by Dempster when he presented the DST. The main characteristic of Dempster Rule is that it is a pure conjunctive rule, it means, that it ignores the conflict information and only combine the common information among sources through a factor K [30]. This factor represent the basic probability mass associated with the conflict. The combination is calculated as follow:

$$bpa(A) = \frac{\sum_{\gamma_i \cap \Omega = A, \gamma_i \in U} bpa(\gamma_i)}{1 - K} \text{ when } A \neq \emptyset \quad (11)$$

$$bpa(\emptyset) = 0 \quad (12)$$

$$K = \sum_{\gamma_i \cap \Omega = \emptyset, \gamma_i \in U} bpa(\gamma_i) \quad (13)$$

Where $bpa(A)$ is the bpa of the resulting interval, $bpa(\gamma_i)$ is the bpa of the intervals form the different sources involved in A, and K is the bpa associated with conflict.

On the other hand, the Mixing rule (also known as p-averaging or averaging) indicates the frequency of the possible values in a range of possible values, generalizing the averaging for probability distributions of probability theory. [30]. This rule behaves as it does probability theory, combining the intervals as probability distributions, obtaining a final structure similar to that obtained averaging those distributions. The results given by this rule is different that with other combination rules, generally giving wider intervals than Dempster rule [30]. The expression for this rule is:

$$bpa_{1\ldots n}(A) = \frac{1}{n} \sum_{i=1}^{n} w_i bpa_i(A) \quad (14)$$

where $bpa_i(A)$ if the bpa associated with the interval A, w_i is a weight related to the reliability of the source and n is the number of sources/experts. Since the aim of these scenarios is to compare the effects on the selection of the combination rule, both experts are considered equally reliable and bpa are distributed uniformly among intervals in each source of information in both scenarios and both rules.

In Figure 9, it can be see a scheme of the geometry of both scenarios. The grey circle represents the combined hard body on the B-plane. Arrows are the interval in vertical and horizontal miss distance, and dash ellipses represent the average position uncertainty ellipsoid projected on the B-plane of the interval given by the expert. Each set of vertical arrow, horizontal arrow and dash ellipse is a combination of the miss distance and position uncertainty intervals given by the experts. Blue sets are linked to Expert 1, while grey sets with Expert 2. Figure 9 (a) shows the scenario of high conflict, since intervals from different sources barely overlap, while Figure 9 (b) shows the low conflict scenario and a bigger overlap can be seen. Table 7 summarize the intervals selected in each scenario.

Table 7: Intervals given by experts on both high conflict scenario and low conflict scenario. All data in meters.

	High Conflict	**Low Conflict**
Expert 1	$\mu_x = [3.0, 5.0], [4.5, 6.0]$	[3.0,5.0], [4.5,6.0]
	$\mu_y = [0.0, 1.0], [3.0, 4.0]$	[0.0,1.0], [3.0,4.0]
	$\sigma_x = [2.0, 4.0], [1.5, 3.5]$	[2.0,4.0], [1.5,3.5]
	$\sigma_y = [1.0, 1.1]$	[1.0,1.1]
Expert 2	$\mu_x = [5.5, 7.0], [6.0, 8.0]$	[4.0,5.5], [5.0,6.5]
	$\mu_y = [1.0, 3.5], [0.5, 2.0]$	[0.5,3.5], [2.5,4.5]
	$\sigma_x = [3.5, 7.0], [3.8, 6.0]$	[2.0,3.5], [1.0,3.5]
	$\sigma_y = [1.05, 1.12]$	[1.05,1.12]

Both rules lead to different combined intervals, generally, wider for Mixing rule and bpa associated to them. The higher the conflict, the more different the combined intervals depending on the rule used. Since Dempster rule tends to ignore the conflict, when it is high, the intervals obtained tends to be narrower compare to those obtain by the Mixing rule. Since the intervals obtained are different, so it is the Belief and Plausibility for P_C. Figure 10 shows these curves. Figure (a) shows the great different between curves obtain for the high conflict case, where Dempster rule gives a narrower intervals with fewer steps. Figure (b) presents the other case, where both curves present a similar trend, despite Dempster rule being slightly narrower. An extreme case can be found when the conflict is so high there is no overlap on the intervals given by the experts, when Dempster Rule cannot be used. In order to overcome this problem, several rules have been proposed [30]. In this paper, no further work on combination rules has been done, since the aim was showing the relevance on the selection of the combination rule. For future works, the search of the best rule or set of rules for this problem, regarding the characteristics of the

intervals given by the experts, is suggested.

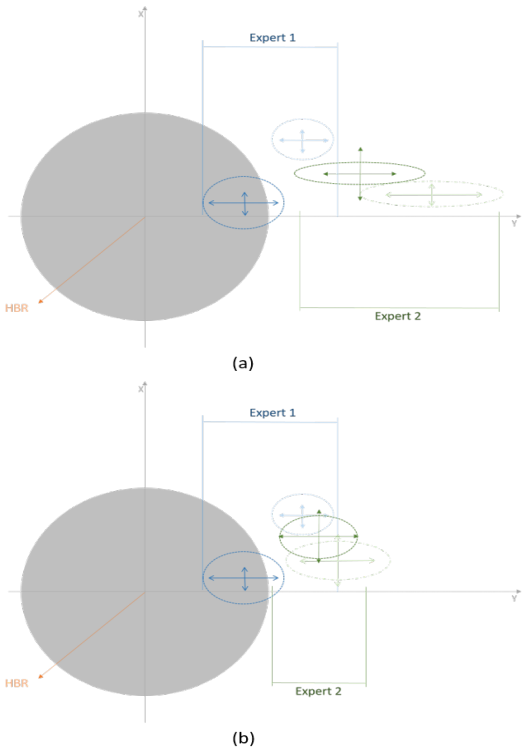

Fig. 9: Geometry of the scenarios. Each set of vertical arrow, horizontal arrow and dash ellipses is an set of intervals given by the sources. Blue sets are Expert 1's intervals and green sets are Expert 2's intervals. Grey circumference is the combine HBR. (a) High conflict. (b) Low conflict.

Illustration of Theory of Evidence on P_C analysis

To illustrate the new method to evaluate the risk of collision using the DST theory, three new scenarios are presented. All those three scenarios present a common geometry, which can be seen in Figure 11, where the intervals given by one of the experts suggest a non probable collision, where the miss distance values are significantly higher than the HBR, while the other leads to a probable collision, with miss distance values close to the HBR. Moreover, information given by the second expert present small values of standard deviation, what in classic probability theory is understood as high quality data, but not necessarily here, while first expert's intervals show a higher values of standard deviation. The difference among scenarios is the reliability given to each expert, what means, the way the epistemic uncertainty coming from the sources is quantified. In the first scenario, both sources are equally trustworthy, in the second scenario, Expert 1 is given a higher level of reliability

Table 8: Intervals given by experts for the three scenarios. All data in meters. Scenario 1: 50-50% reliability. Scenario 2: 95-5% reliability. Scenario 3: 5-95% reliability.

	Expert's intervals
Expert 1	$\mu_x = [15.0, 18.0], [16.5, 25.0]$ $\mu_y = [0.0, 1.0], [0.1, 1.1]$ $\sigma_x = [10.0, 14.0], [7.0, 11.0]$ $\sigma_y = [1.0, 1.1]$
Expert 2	$\mu_x = [3.0, 5.0], [3.0, 7.0], [6.0, 10.0]$ $\mu_y = [0.0, 1.5], [0.5, 1.0], [1.4, 1.6]$ $\sigma_x = [1.0, 1.5], [0.5, 2.0], [2.0, 5.0]$ $\sigma_y = [1.05, 1.12]$

compare with Expert 2, while in the third scenario is the opposite: Expert 2 is more reliable. Table 8 summarize the three cases. Since the intervals giving by both experts are disjoint (high conflict), Dempster rule cannot be applied, so Mixing is the combination rule used in all three scenarios.

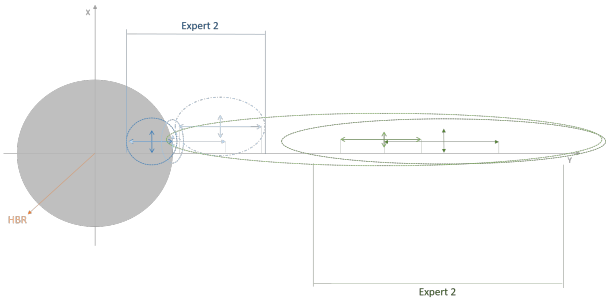

Fig. 11: Geometry of the three scenarios. Each set of vertical arrow, horizontal arrow and dash ellipses is an set of intervals given by the sources. Blue sets are Expert 1's intervals and green sets are Expert 2's intervals. Grey circumference is the combine HBR.

In Figure 12, the Plausibility and Belief curves for the Probability of Collision for the three scenarios are shown. There, it can be seen how drastically the confidence on a value of the P_C can vary depending on the reliability of the source of information, even if the same intervals are used and the same aleatory uncertain (standard deviation) is considered. It is in theses situation where the effect of the epistemic uncertainty can be highlighted.

When both sources are equally reliable, Figure 12 (a), the confidence on values of P_C greater than 0.15 is lower than 50%. It means that, from the evidence, there is no great support on the fact that a collision will happen with a probability greater than that value. Moreover, since the gap between Belief and Plausibility remains small for almost all values, it

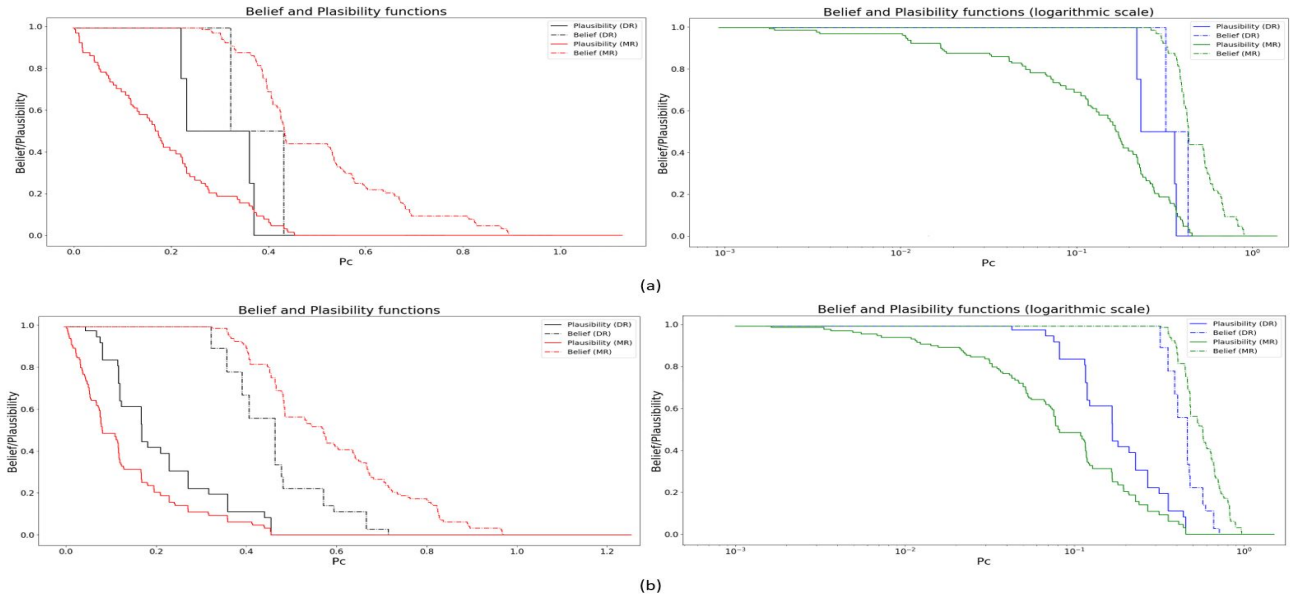

Fig. 10: Belief and Plausibility curves using combination rules. Right: lineal scale; Left: logarithmic scale. Red and green lines: Mixing rule; Black and blue lines: Dempster rule; Solid lines: Plausibility curves. Dash lines: Belief curves. (a) High conflict scenario. (b) Low conflict scenario.

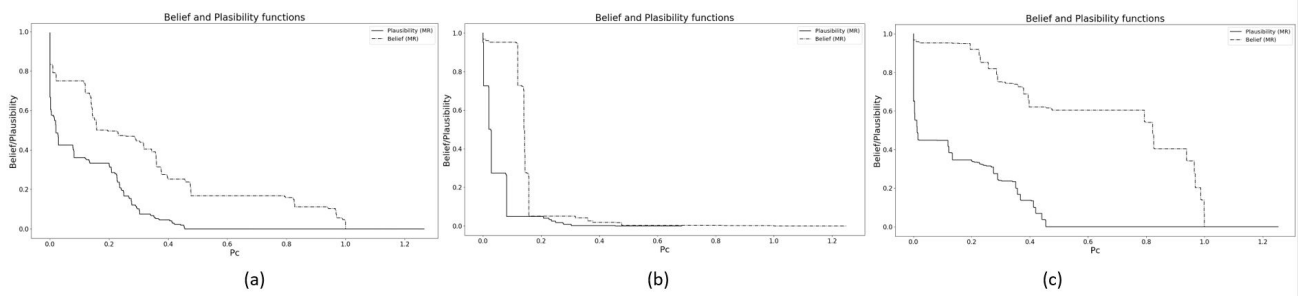

Fig. 12: Plausibility and Belief of P_C for the three scenarios. (a) Scenario 1: Experts equally reliable. (b) Scenario 2: Expert 1 more reliable than Expert 2. (c) Scenario 3: Expert 2 more reliable than Expert 1. Solid lines: Plausibility curves; Dash lines: Belief curves.

means that evidence provided is enough to take a confident decision. Moving to Figure 12 (b), since evidences provided by Expert 1, which suggested a less probable encounter, are more trustworthy, there is almost no support from evidence that probability of collision is bigger than 0.15. Even if one of the experts suggests a more likely conjunction event, since the information it provides is less reliable, the final decision leads to a high confidence on a collision not to happen. From an operator's point of view, if a threshold is set between $P_{C_0} = 0.15$ and $P_{C_0} = 0.2$, while the first situation could lead to a possible action if a very conservative behaviour is followed, the second scenario clearly points to a decision where no action is the best option.

The opposite occurs on Scenario 3 (Figure 12 (c)). Here, Expert 2 is more reliable and, as a consequence, there is more support on the idea of a P_C greater than 0.15. Actually, the Belief associated to values of P_C up to 0.8 is higher than 0.6, what present a very different situation than in the previous cases. If and operator is using a threshold of $P_{C_0} = 0.15$, there is a great support on that assumption and, at the same time, there is lack of evidence against it, or what it is the same, the Belief is high while the Plausibility

is low. In this situation, the decision of taking any action to reduce P_C seems to be the best idea. Something different happens if the threshold is set to values of P_C between 0.5 and 0.8. In a situation like that, while there is evidence that P_C is greater than that value (Belief greater than 0.5), at the same time, there is evidence against the proposition (Plausibility near to zero). Such scenario is representative of a situation where the available information is not enough to take a confident decision. If it is not possible to obtain more reliable data, the operator can choose for either a conservative behaviour, since there is some evidence that suggests a high P_C, and take further actions to reduce it, or a less conservative approach and decide not to take any actions, since there also high degree of evidence against the fact that P_C takes high values. A similar situation could be found on Scenario 2 if threshold is between 0.05 and 0.15. Different factor can influence the operator's decision, like the cost of the maneuver compare to the cost of the satellite, the risk a CAM involves, the likely of a future collision... Further works to develop a decision-making system to support operator is suggested.

6. Conclusions

This paper presents a novel Artificial Neural Network-based system to support decision making in the context of STM. The system is able to predict the evolution of the equinoctial parameters of the space debris bodies as well as the B-parameter, MOID and Probability of Collision between them and the primary satellite in a given interval of time given the initial orbital parameters. All variables are predicted with high level of accuracy during the whole interval of time. The system have shown its utility as a tool to predict potential encounters between and operative satellite and a set of pieces of space debris with high accuracy and efficiency. In addition of its precision and speed, other advantage is the not used of dynamic models since it is a sample-based system, what also allowed to improved accuracy when more data are available. All these characteristic are desirable in a environment where space population is rapidly increasing and the trend leads to the automation of systems.

This paper also introduces a new formulation to evaluate the risk of collision for conjunction events where epistemic uncertainty on satellite's position is included. Unlike previous methods where epistemic uncertainty is treated as an aleatory variable, the new formulation used concepts from Dempster-Shafer's Theory of Evidence to account for epistemic uncertainty. Different scenarios have been presented to show how the concepts of Belief and Plausibility leads to intervals of confidence for P_C used for decision-making.

The contributions presented here leave issues to be addressed in future works, including:

- The introduction of some improvements ototthe ANN-system, predicting also the pertubed primary satellite movement, allowing different initial time for the space debris object's' equinoctial parameters, using real data for training...
- The systematic analysis of ANN hyper-parameter, in order to optimize them in the context of this problem.
- The use of other AI techniques on the system, to better understand the potential of this methods.
- A better understanding of he concepts introduce from Theory of Evidence in conjunction risk assessment.
- The removal of assumptions used in this paper, like normality and uncorrelation of uncertainty and independence of sources.
- Combination of both ideas along with the proposed risk assessment system in order to, eventually, automatize the conjunction prediction and the decision-making, taking into account cost of current and future maneuvers, risk of them, cost of satellite...

References

[1] "ESA's Annual Space Environment Report". In: *ESA Space Debris Office, ESOC-ESA* GEN-DB-LOG-00271-OPS-SD.3.2 (July 2019).

[2] S. Le May et al. "Space debris collision probability analysis for proposed global broadband constellations". In: *Acta Astronautica* 151 (2018), pp. 445–455.

[3] H. Lewis et al. *Sensitivity of the space debris environment to large constellations and small satellites*. 2017.

[4] P.G. Michael. "Establishing space traffic management standards, guidelines, and best practices". In: *Aerospace Corporation* (Sept. 2019).

[5] T. Kelso. "Iridium33/Cosmos2251 Collision". In: (July 2009). URL: http://celestrak.com/events/collision/.

[6] ESA. "ESA spacecraft dodges large constellation". In: (). URL: https://www.esa.int/Our_Activities/Space_Safety/ESA_spacecraft_dodges_large_constellation.

[7] H. Peng and X. Bai. "Exploring Capability of Support Vector Machine for Improving Satellite Orbit Prediction Accuracy". In: *Journal of Aerospace Information Systems* 15.6 (2018), pp. 366–381.

[8] M. Vasile et al. "Artificial Intelligence in Support to Space Traffic Management". In: *68th International Astronautical Congress, Adelaide, Asutralia* (Sept. 2017).

[9] D. Izzo, M. Märtens, and B. Pan. "A survey on artificial intelligence trends in spacecraft guidance dynamics and control". In: *Astrodynamics* 3.4 (Dec. 2019), pp. 287–299.

[10] Hao Peng and Xiaoli Bai. "Artificial Neural Network–Based Machine Learning Approach to Improve Orbit Prediction Accuracy". In: *Journal of Spacecraft and Rockets* 55.5 (2018), pp. 1248–1260.

[11] R. Patera. "General Method for Calculating Satellite Collision Probability". In: *Journal of Guidance Control and Dynamics - J GUID CONTROL DYNAM* 24 (July 2001), pp. 716–722.

[12] R. Serra et al. "Fast and Accurate Computation of Orbital Collision Probability for Short-Term Encounters". In: *Journal of Guidance, Control, and Dynamics* 39 (Jan. 2016), pp. 1–13.

[13] S. Alfano. "Review of conjunction probability methods for short-term encounters". In: *Advances in the Astronautical Sciences* 127 (Jan. 2007), pp. 719–746.

[14] M. Balch, R. Martin, and S. Ferson. "Satellite conjunction analysis and the false confidence theorem". In: *Proceedings of the Royal Society A: Mathematical, Physical and Engineering Sciences* 475 (July 2019).

[15] G. Shafer. *A mathematical theory of evidence*. Princeton University Press, 1976.

[16] G. Cybenko. "Approximation by superpositions of a sigmoidal function". In: *Mathematics of Control, Signals and Systems* 2.4 (Dec. 1989), pp. 303–314.

[17] W. Duch and N. Jankowski. "Survey of Neural Transfer Functions". In: *Neural Computing Surveys* 2 (1999), pp. 163–212.

[18] P.L. Rosin and F. Fierens. "Improving neural network generalisation". In: *1995 International Geoscience and Remote Sensing Symposium, IGARSS '95. Quantitative Remote Sensing for Science and Applications* 2 (July 1995), pp. 1255–1257.

[19] M. T. Hagan and M. B. Menhaj. "Training Feedforward Networks with the Marquardt Algorithm". In: *Trans. Neur. Netw.* 5.6 (Nov. 1994), pp. 989–993.

[20] D.C. Psichogios and L.H. Unga. "A Hybrid Neural Network - First Principles Approach to Process Modeling". In: *AIChE Journal* 38 (10 Oct. 1992), pp. 1499–1511.

[21] G.F. Gronchi. "On the Stationary Points of the Squared Distance between Two Ellipses with a Common Focus". In: *Siam Journal on Scientific Computing* 24 (Aug. 2002).

[22] G.F. Gronchi. "An Algebraic Method to Compute the Critical Points of the Distance Function Between Two Keplerian Orbits". In: *Celestial Mechanics and Dynamical Astronomy* 93.1 (Sept. 2005), pp. 295–329. ISSN: 1572-9478.

[23] M. Jah. "Derivation of the B-plane (Body Plane) and Its Associated Parameters". In: *Jet Propulsion Lab* (2002).

[24] D.A. Vallado. "Fundamentals of Astrodynamics and Applications". In: *The Space Technology Library. Fourth Edition* (2013), pp. 961–964.

[25] L. Newman et al. "Evolution and Implementation of the NASA Robotic Conjunction Assessment Risk Analysis Concept of Operations". In: *Advanced Maui Optical and Space Surveillance Technologies Conference* (Sept. 2014).

[26] S. Alfano and D. Oltrogge. "Probability of Collision: Valuation, variability, visualization, and validity". In: *Acta Astronautica* 148 (Apr. 2018).

[27] J. C. Helton. "Uncertainty and sensitivity analysis in the presence of stochastic and subjective uncertainty". In: *Journal of Statistical Computation and Simulation* 57 (1997), pp. 3–76.

[28] W.L. Oberkampf and J.C. Helton. "Investigation of Evidence Theory for Engineering Applications". In: *AIAA 2002-1569, Denver Colorado*. 4th Non-Deterministic Approaches Forum. 2002.

[29] P. Soundappan et al. "Comparison of evidence theory and Bayesian theory for uncertainty modeling". In: *Reliability Engineering System Safety - RELIAB ENG SYST SAFETY* 85 (July 2004).

[30] K. Sentz and S. Ferson. *Combination of Evidence in Dempster-Shafer Theory*. Jan. 2002.